NASA TECHNICAL NOTE

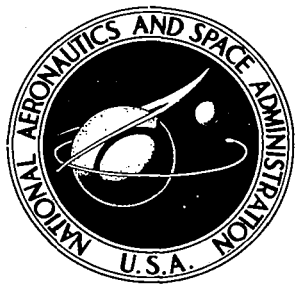

NASA TN D-6764

COMPARISON OF PREDICTED AND EXPERIMENTAL HEAT-TRANSFER AND PRESSURE-DROP RESULTS FOR AN AIR-COOLED PLUG NOZZLE AND SUPPORTING STRUTS

by Edwin J. Graber, Jr., and John S. Clark

Lewis Research Center
Cleveland, Ohio 44135

NATIONAL AERONAUTICS AND SPACE ADMINISTRATION • WASHINGTON, D. C. • APRIL 1972

1. Report No. NASA TN D-6764	2. Government Accession No.	3. Recipient's Catalog No.
4. Title and Subtitle COMPARISON OF PREDICTED AND EXPERIMENTAL HEAT-TRANSFER AND PRESSURE-DROP RESULTS FOR AN AIR-COOLED PLUG NOZZLE AND SUPPORTING STRUTS		5. Report Date April 1972 6. Performing Organization Code
7. Author(s) Edwin J. Graber, Jr., and John S. Clark		8. Performing Organization Report No. E-6709
9. Performing Organization Name and Address Lewis Research Center National Aeronautics and Space Administration Cleveland, Ohio 44135		10. Work Unit No. 764-74 11. Contract or Grant No.
12. Sponsoring Agency Name and Address National Aeronautics and Space Administration Washington, D.C. 20546		13. Type of Report and Period Covered Technical Note 14. Sponsoring Agency Code
15. Supplementary Notes		

16. Abstract

A calculational procedure is presented to analyze the heat-transfer and fluid-flow characteristics of a convectively air-cooled plug nozzle for a supersonic afterburning turbojet engine. An approximate method was used to calculate hot-gas stream properties for low nozzle-pressure ratios. Both an integral boundary-layer technique and a simple pipe-flow equation were used to calculate the hot-gas to plug-wall heat-transfer coefficients.

17. Key Words (Suggested by Author(s))

Nozzle
Plug nozzle
Cooling
Heat transfer
Convection
Fluid flow
Supersonic

18. Distribution Statement

Unclassified - unlimited

19. Security Classif. (of this report)	20. Security Classif. (of this page)	21. No. of Pages	22. Price*
Unclassified	Unclassified	38	$3.00

* For sale by the National Technical Information Service, Springfield, Virginia 22151

COMPARISON OF PREDICTED AND EXPERIMENTAL HEAT-TRANSFER AND PRESSURE-DROP RESULTS FOR AN AIR-COOLED PLUG NOZZLE AND SUPPORTING STRUTS

by Edwin J. Graber, Jr., and John S. Clark

Lewis Research Center

SUMMARY

A calculational procedure is presented to analyze the heat-transfer and fluid-flow characteristics of a convectively air-cooled plug-nozzle operating on an afterburning turbojet engine. Anderson's method was used to predict hot-gas static pressures in the supersonic stream with fully expanded flow (high nozzle-pressure ratios); the results were excellent. For low nozzle-pressure ratios, the flow was assumed to expand one-dimensionally and isentropically to the plug back pressure. Wall temperatures predicted using this latter pressure distribution agreed well with the wall temperatures predicted using the measured hot-gas pressures (maximum deviation was about 30 K (54° R)).

Either an integral boundary-layer technique or a simple pipe-flow equation may be used to calculate convective heat transfer from the hot gas to the wall. The simple pipe-flow equation results in the prediction of slightly higher wall temperatures than does the integral technique. Experimental wall temperatures were generally in good agreement with the two predicted wall temperature distributions.

Excellent agreement was noted between measured and predicted coolant static-pressure distributions. The plug-coolant temperature rise was generally overpredicted by about 22.2 K (40° R); possible explanations are offered.

Although an analysis of the struts, which support the plug, was purposely kept simple, reasonable results were obtained. Potential flow over an ellipse was used to calculate hot-gas static pressure; the results were satisfactory.

INTRODUCTION

An analytical model is presented for the prediction of temperature and pressure distributions of a convectively air-cooled plug nozzle (and supporting struts) operating on an

afterburning turbojet engine. Reference 1 described the nozzle and test and presented some preliminary experimental results. Comparisons of predictions and experimental data are presented herein.

The plug nozzle was selected for this study since in preliminary tests (ref. 2) it had exhibited high performance characteristics over a wide range of operating conditions. In addition, static jet noise tests indicate that the plug is slightly quieter than ejector nozzles (ref. 3). A cooling system is required for the plug and its attachment struts during afterburning because they are immersed in the hot exhaust gases. The cooling system analyzed herein employs parallel-flow convection cooling with either compressor discharge air or facility air as the coolant. This system was designed to maintain wall temperatures below 1220 K (2200° R) when subjected to 1945 K (3500° R) exhaust gases using up to $3\frac{1}{2}$ percent of the engine primary air for cooling. Since engine cycle efficiency is reduced when air is taken from the compressor, the plug cooling requirement must be minimized.

Plug and strut outer wall temperatures, coolant pressures, coolant temperatures, and their surrounding hot-gas pressure and temperature distributions were calculated using the prediction techniques presented in this report. These pressures and temperatures are compared with experimental data acquired in tests conducted in an altitude simulation chamber at the Lewis Research Center. For these tests, the plug nozzle was installed on a J-85 afterburning turbojet engine. Details of the test facility and test conditions are given in reference 1; only a brief description follows.

APPARATUS AND TEST CONDITIONS

The nozzle configuration tested consisted of a 10° half-angle conical plug, truncated at 60 percent of the distance between the primary throat and the end of a full conical plug. The plug was attached to the nacelle of a J-85-13 GE turbojet engine upstream of the primary nozzle. The plug was 40.6 centimeters (16 in.) at its maximum diameter, and the secondary shroud was 63.5 centimeters (25 in.) in diameter. The struts that support the plug were approximately elliptical in cross section with major and minor axes of 14 centimeters (5.5 in.) and 6.3 centimeters (2.5 in.), respectively. Figure 1 shows a schematic diagram of the plug, afterburner liner, engine nacelle, and facility exhaust collector as installed on the engine in the propulsion systems laboratory at the Lewis Research Center.

A translating secondary shroud is required to maintain efficient nozzle thrust performance over a range of nozzle pressure ratios by varying the hot-gas expansion area ratio. The translating shroud was simulated in these tests by a series of fixed-length shrouds. Most of the testing was done with the longest shroud (38.1 cm (15 in.) beyond the primary throat) for high pressure ratios and with a shorter shroud (10.1 cm (4 in.)

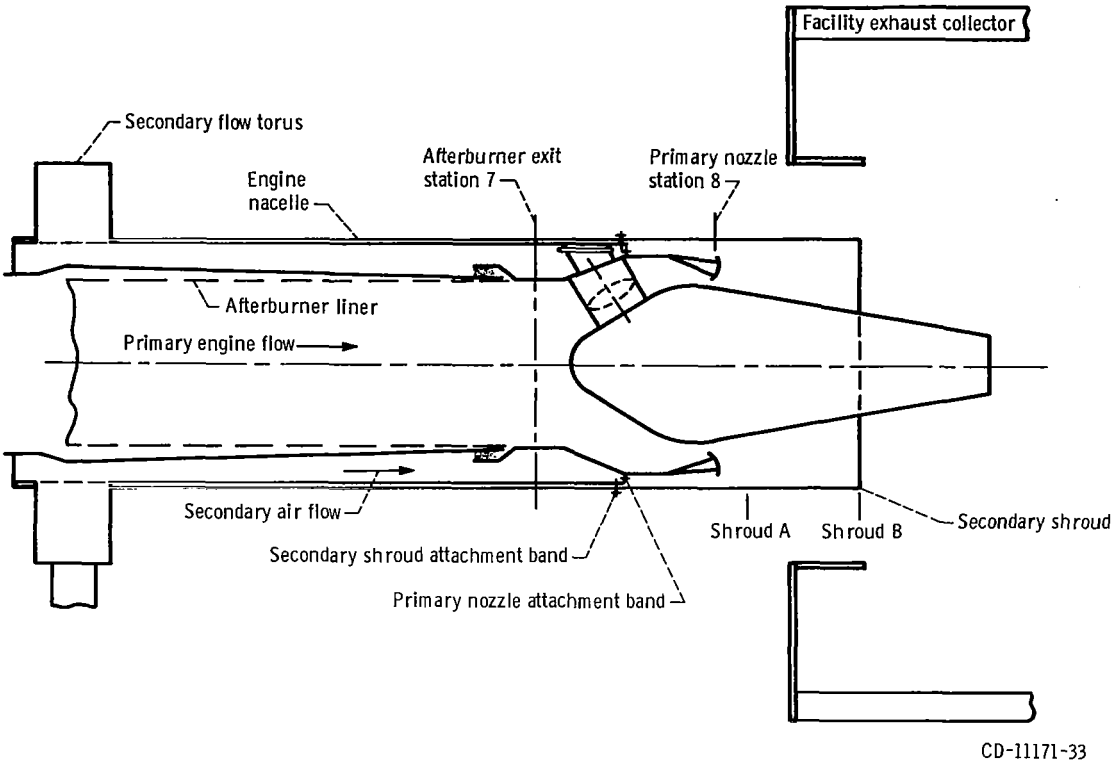

Figure 1. - Schematic diagram of nozzle test configuration.

beyond the primary throat) for transonic pressure ratios. The ends of these two shrouds are indicated in figure 1 and are designated as shrouds A and B. An even shorter shroud should be used for maximum performance at takeoff (ref. 4).

Similarly, a variable-iris primary nozzle, which is required to allow changes in engine-operating conditions (afterburner level, for example), was simulated by a series of fixed area nozzles. Only results obtained for the largest primary nozzle area, corresponding to the highest gas temperatures, are presented in this report.

The plug and strut cooling scheme is shown schematically in figure 2. Strut and plug cooling air enters the struts near the engine nacelle and makes its way radially inward toward the plug in the passage labeled "strut coolant inlet" in section A-A of figure 2. This passage is capped to prevent the coolant from dumping directly inside the plug. The coolant flows from the strut coolant inlet passage into the strut leading-edge plenum through a series of holes. From the leading-edge plenum, the cooling air then flows through another series of staggered holes into the finned axial coolant channels. The axial coolant channels were formed by attaching 0.0508-centimeter (0.020-in.) thick fins (Nickel 200) to the strut outer wall (Inconel 625) (of thickness, 0.157 cm (0.062 in.)). The fins are 0.635 centimeter (1/4 in.) long and spaced 0.317 centimeter (1/8 in.) apart

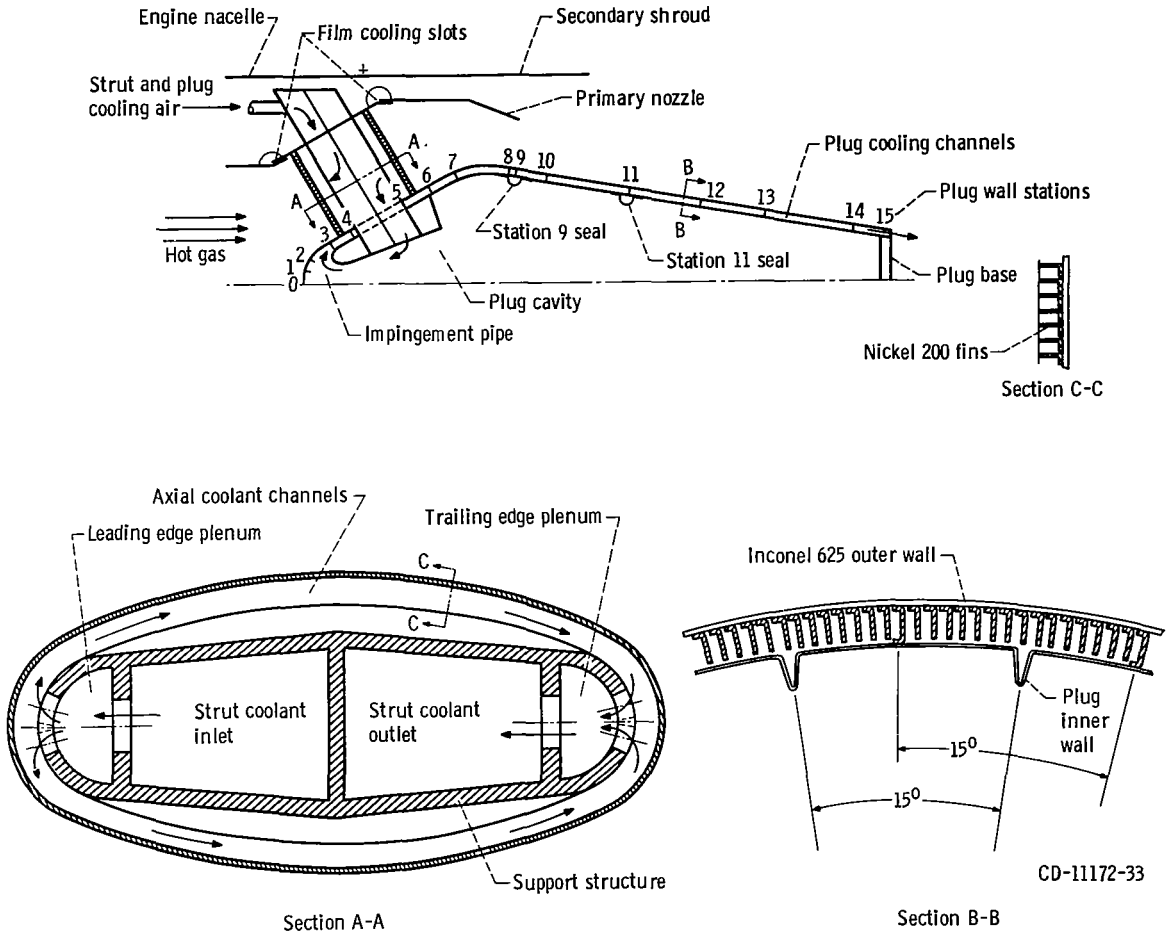

Figure 2. - Strut and plug internal convection cooling configuration.

(see section C-C of fig. 2). The cooling air flows between the nickel fins around the strut to the strut trailing edge.

The flow pattern at the trailing edge is essentially the same as the leading edge with the flow direction reversed. The air passes from the coolant channels, through a staggered hole arrangement into the trailing edge plenum, and through larger holes into the strut coolant outlet passage. The air then flows radially inward through an opening in the strut support and into the plug cavity.

The plug cavity is closed at the plug base; the coolant is therefore forced forward toward the plug leading edge and through a venturi passage where it impinges on the inside of the plug leading edge. The cooling air then enters the plug cooling channels, which are made of 0.0813-centimeter (0.032-in.) thick fins (Nickel 200) attached to the 0.157-centimeter (0.062 in.) outer wall (Inconel 625). The plug fins, shown in section B-B of

figure 2, are 0.794 centimeter (5/16 in.) long, and the circumferential spacing varies, depending on position along the length of the plug surface.

Also shown in figure 2 are the plug stations 0 to 15. The number of fins between each of the plug stations is shown in table I. The number of fins and, hence, fin spacings, were selected to yield approximately uniform plug wall temperatures at the maximum heat load condition.

TABLE I. - NUMBER OF FINS ALONG PLUG

Station	Number of fins	Station	Number of fins
0-1	6	8-9	360
1-2	6	9-10	288
2-3	72	10-11	264
3-4	144	11-12	216
4-5	192	12-13	216
5-6	240	13-14	144
6-7	336	14-15	120
7-8	360		

The inner coolant channel was completed by attaching the 0.0254-centimeter (0.010-in.) inner wall to the fins. The inner wall was brazed to the fins at one end to allow for differential axial thermal expansion between the inner and outer walls. Differential circumferential expansion was compensated for by including bellows joints in the inner wall.

Also shown in figure 2 are the plug station 9 and 11 seals. A mineral wool rope type of packing was inserted beneath the retaining clips; the inner wall from the adjacent section was inserted, during assembly, between the nickel fins and the mineral wool rope (details shown in ref. 1). Thus, it was hoped that even with relative motion caused by thermal expansion between the inner and outer walls at that point, the seal would minimize cooling air leakage from the higher pressure interior of the plug to the cooling channels. After assembly and subsequent checking, it was found that the seal permitted a rather large coolant leak at stations 9 and 11, and these seals had to be augmented with a high-temperature synthetic rubber sealant. A discussion of the magnitude of this leak is presented in reference 1.

The primary nozzle was film cooled with residual cooling from the afterburner liner and two film-cooling slots. One of these slots was installed just upstream of the struts, and the other just downstream of the struts. Secondary air also convectively cooled the primary nozzle to some extent. The secondary shroud was film cooled with the secondary air flow. Although much film-cooling data were obtained in this series of tests, this report will be limited to the convective cooling analysis of the struts and plug.

The nozzle was tested over the following range of conditions. (Symbols are defined in appendix A):

Exhaust gas total pressure, P_8, atm	1 to 3
Exhaust gas total temperature, T_8, K; ^{o}R	556 to 1860; 1000 to 3350
Nozzle pressure ratio, P_8/p_0	2 to 100
Plug coolant flow rate, percent of primary	2 to 5
Throat areas (nominal), cm^2; $in.^2$:	
1	742; 115
2	873; 135
3	1130; 175
Secondary shroud lengths (measured from primary throat), cm; in.:	
1	-12.7; -5
2	10.1; 4
3	17.8; 7
4	25.4; 10
5	38.1; 15
Engine flow rate, kg/sec; lbm/sec	9.07 to 22.68; 20 to 50

A series of tests was run using facility cooling air, and a series of tests was run using cooling air obtained from the engine compressor discharge ports. A schematic of the test installation is shown in figure 3.

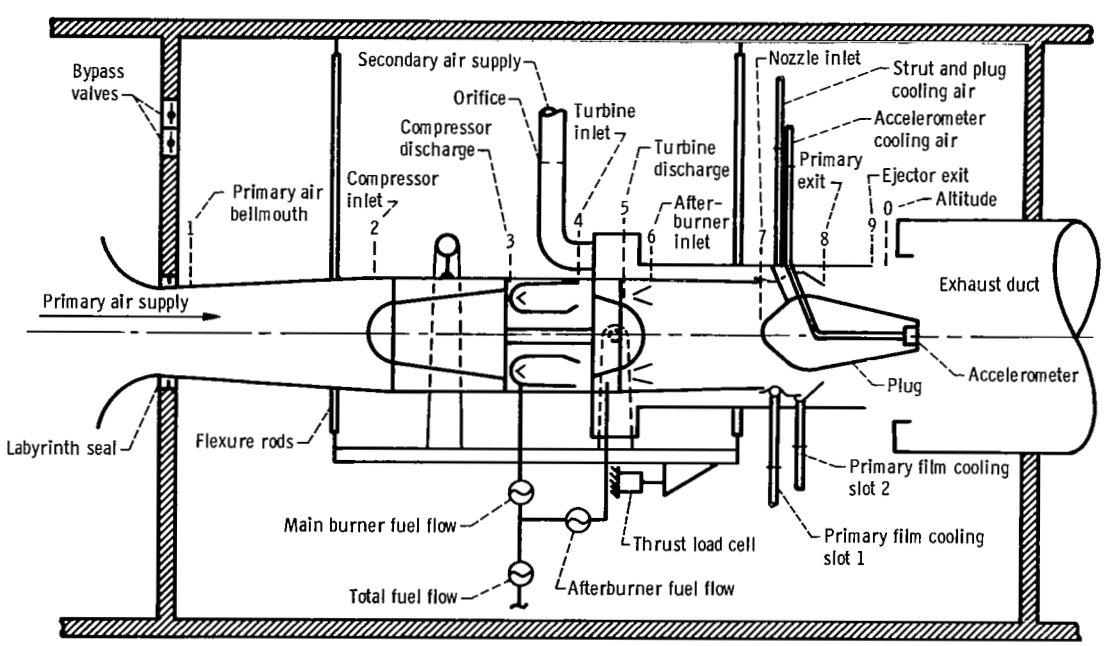

Figure 3. - Test installation.

PREDICTION TECHNIQUE

For prediction purposes, the plug and struts were divided into a series of axisymmetric nodes. Using either one-dimensional isentropic flow equations or a prediction method developed by Anderson (ref. 4), the hot-gas velocity, temperature, and pressure distributions were calculated. Then, assuming a one-dimensional energy balance between the hot gas and coolant for each node (note that axial conduction was not considered), the heat transferred to the coolant at each nodal junction was calculated. The calculations began at the initial upstream node where the coolant inlet total temperature and mass flow rate were known. Heat was continually added to the coolant in discrete quantities at the downstream junction of each node, resulting in an increasing total temperature.

After calculating the coolant total temperature distribution, the coolant static pressure, Mach number, and static temperature distributions were calculated. These calculations started at the choked plug coolant passage exit (station 15). The static pressure was calculated using the calculated coolant exit temperature in the choked flow equation of Fleigner (ref. 5). The coolant pressure distribution was then calculated using the integrated form of the momentum equation (ref. 6) to calculate the pressure change between adjoining nodes. To calculate the coolant total temperatures used in the momentum equation, an energy balance was required between the hot-gas recovery temperature and the coolant recovery temperature. Since the recovery temperature depends on the local Mach number, an iteration was required on the coolant side to calculate the recovery temperature. On the first iteration the total temperature was used as the recovery temperature. Usually convergence was obtained on the second iteration.

It should be noted that coolant pressure losses from the compressor bleed ports to the strut inlet cavity were not calculated. These pressure losses were considered to be peculiar to each engine application and not part of a general plug analysis.

Plug Model

Hot-gas pressure, velocity, and temperature distributions. - Upstream of the nozzle throat, the hot-gas pressure, velocity, and static-temperature distributions were calculated using isentropic flow relations, in conjunction with the known mass flow rate, total pressure, total temperature, and local- to throat-area ratios. Beyond the throat (supersonic flow) for high nozzle-pressure ratios (i.e., $P_8/p_0 \geq 10$) a procedure developed by Anderson (ref. 4) was used to determine the local flow characteristics, and for low nozzle-pressure ratios (i.e., $P_8/p_0 < 10$) the isentropic flow relations were used. For the low pressure ratio cases, the hot gas was assumed to isentropically expand to the

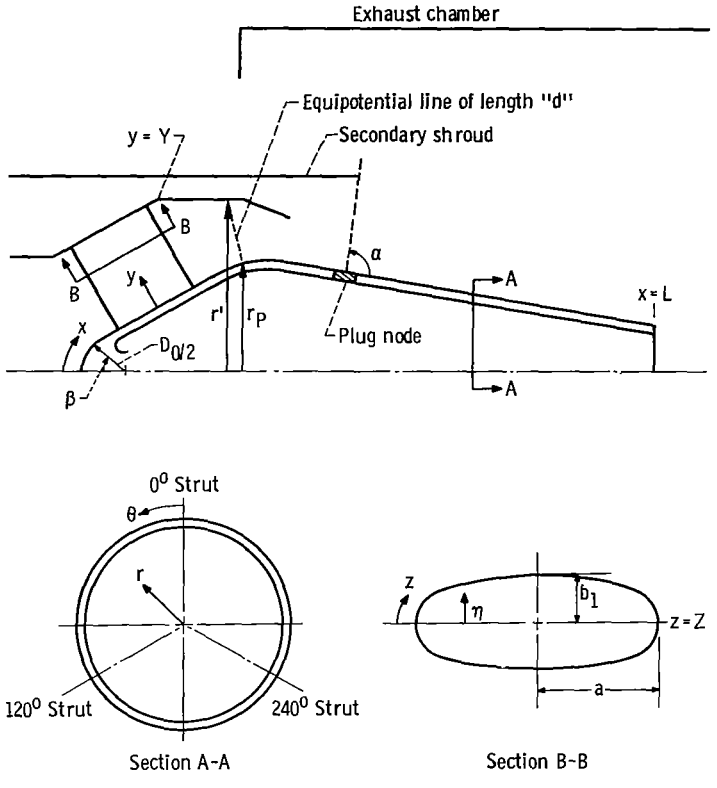

Figure 4. - Plug nozzle coordinate system.

back pressure. It was also assumed that the hot gas did not separate from the plug surface throughout the flow field. For details of the calculation procedure see reference 7.

Hot-gas-side heat-transfer coefficient. - Up to the surface position $x/L = 0.09$ ($\beta \simeq 59^o$ in fig. 4) the hot-gas-side heat-transfer coefficient was the larger of the following two heat-transfer coefficients:

(1) An equation for predicting an average heat-transfer coefficient for flow over a sphere (ref. 8) was adjusted to a local value in the same manner as recommended for flow over a cylinder (ref. 8). The following expression for the local heat-transfer coefficient resulted:

$$h_g = 0.37\left(\frac{k_g}{D_0}\right)Re_{D_0,g}^{0.6}\,Pr_g^{0.4}\left[1-\left(\frac{\beta}{90}\right)^3\right] \qquad (1)$$

The diameter D_0 is the diameter of the plug leading-edge region (see fig. 4). Equation (1) is in good agreement with the data of reference 9.

(2) For flow in a nozzle, Bartz (ref. 10) recommended the pipe-flow equation

$$h_g = 0.026\, Re_g^{0.8} Pr_g^{0.4} \frac{k_g}{D_{H,g}} \tag{2}$$

Beyond $x/L = 0.09$ the hot-gas-side h was either the Bartz-Boldman coefficient calculated using an integral boundary-layer method (ref. 11) or the pipe-flow coefficient given by equation (2). The fluid properties of equations (1) and (2) were evaluated at the Eckert reference temperature (ref. 6).

$$T_r = 0.5\, T_{w,i} + 0.28\, t_c + 0.22\, T_{c,rec} \tag{3}$$

The Reynolds number in equation (2) was based on the hydraulic diameter

$$D_{H,g} = \frac{4A}{\mathscr{P}} \tag{4}$$

In terms of the nomenclature of figure 4, the flow cross-sectional area A and the wetted perimeter $\mathscr{P}$ used in equation (3) were (a) in the region where struts were present

$$A = \frac{2\pi\left(r_p + r'\right)d}{2} - 3(2\eta d) \tag{5}$$

$$\mathscr{P} = 2\pi\left(r_p + r'\right) - 3(4\eta) + 3(2d) \tag{6}$$

and (b) in the region where no struts were present

$$A = 2\pi \frac{\left(r_p + r'\right)}{5} d \tag{7}$$

$$\mathscr{P} = 2\pi\left(r_p + r'\right) \tag{8}$$

Up to the nozzle throat the outer ratius r' was simply the distance between the plug axis and the primary shroud. Beyond the nozzle throat (primary shroud ends at the throat) flow areas A_g consistent with the previously calculated hot-gas pressures, were calculated using the standard one-dimensional, compressible, isentropic flow relations for supersonic flow of a perfect gas. Then, assuming that the hot gas did not separate from the plug surface, the outer flow radius r' was calculated for an annulus of inner radius r_p, outer radius r', and cross-sectional area A_g.

Radiation heat flux. - The radiation heat flux from the gas flame to the plug wall was calculated as suggested in reference 12:

$$\frac{Q_{rad,fl}}{A_w} = \sigma\left(\frac{\epsilon_w + 1}{2}\right)\epsilon_{fl}t_{fl}^{1.5}\left[t_{fl}^{2.5} - T_{w,o}^{2.5}\right] \tag{9}$$

The emissivity of the flame was given as

$$\epsilon_{fl} = 1 - \exp\left[\frac{-18.5\ P_8(Fa \cdot \xi)^{1/2}}{t_{fl}^{1.5}}\right] \tag{10}$$

and the emissivity of the wall ϵ_w was assumed to be 0.65, which is a reasonable mean value for this material at the temperatures investigated.

The radiation heat flux from the plug to the cool exhauster chamber, which was assumed to be maintained at a constant 311.1 K (100° F), was calculated using the standard equation of reference 8 for radiation between two gray bodies with the chamber area much greater than the wall area:

$$\frac{Q_{rad,ch}}{A_w} = \frac{\sigma\left(T_{w,o}^4 - T_{ch}^4\right)}{\frac{1 - \epsilon_w}{\epsilon_w} + \frac{1}{F_{w-ch}}} \tag{11}$$

In this equation, the shape factor between each nodal element and the exhauster chamber, F_{w-ch}, was approximated by the equation:

$$F_{w-ch} = \frac{1}{2}(1 - \cos\ \alpha) \tag{12}$$

The angle α is shown in figure 4. Equation (12) was derived for two infinitely wide flat plates (one semiinfinite in length and the other of length ΔL).

Radiation from the plug and struts to the afterburner walls and primary nozzle was neglected because these surfaces were all about the same temperature.

The total radiation heat flux to the plug wall was, therefore, expressed as

$$\frac{Q_{rad}}{A_w} = \frac{Q_{rad,fl}}{A_w} - \frac{Q_{rad,ch}}{A_w} \tag{13}$$

Coolant-side heat-transfer coefficient. - As shown in figure 2, the coolant entered the plug inner chamber, passed through an impingement pipe, and impinged on the plug leading edge. It then passed through channels between the plug inner and outer walls and finally exited at the plug trailing edge. Nickel fins were attached to the inner surface of the plug outer wall to increase the heat transfer to the coolant.

For the leading-edge region, the coolant-side heat-transfer coefficient was calculated using a correlation developed by cross-plotting data presented by Gordon and Cobonpue (ref. 13) for a jet impinging on a flat plate with a nozzle-to-plate spacing of 2 diameters or less. This correlation is

$$h_c = 1.465\, Re_c^{0.453} \frac{k_c}{D_{imp}} \tag{14}$$

Since the flow in the finned coolant channels was always turbulent, the heat-transfer coefficient for the channel walls was calculated using (ref. 8)

$$h_c = 0.023\, Re_c^{0.8} Pr_c^{0.4} \left[1 + \left(\frac{D_H}{L}\right)^{0.7}\right] \frac{k_c}{D_H} \tag{15}$$

Entrance region effects were included since a different number of relatively short fins were used in the various sections of the plug in an attempt to produce a uniform outer-wall temperature. An effective heat-transfer coefficient due to the presence of fins was then calculated using

$$h_{c,eff} = \frac{h_c}{S}\left[(S - b) + 2\sqrt{\frac{k_f b}{2h_c}} \tanh\left(l\sqrt{\frac{2h_c}{k_f b}}\right)\right] \tag{16}$$

Thus, the local heat flux to the coolant was expressed as

$$\frac{Q}{A_w} = h_{c,eff}(T_{w,i} - T_{c,rec}) \tag{17}$$

The coolant recovery temperature in equation (17) was calculated using the equation

$$T_{c,rec} = t_c + \sqrt[3]{Pr_c}\,(T_c - t_c) \tag{18}$$

The fluid properties in equations (14) to (16), and (18) were also calculated at the Eckert reference temperature (eq. (3)).

Coolant pressure distribution. - For the impingement-cooled leading edge the loss in total pressure from the impingement pipe to the entrance of the cooling channels was assumed to be one velocity head based on the velocity at the channel inlet (ref. 14).

For the coolant channels the pressure drop between nodes was calculated using the integrated momentum equation for one-dimensional compressible flow in a duct as suggested in reference 6:

$$\Delta p = p_1 - p_2 = \frac{\dot{m}^2}{g_c A_{av}} \left[\frac{1}{\rho_2 A_2} - \frac{1}{\rho_1 A_1} + \frac{4f\,\Delta L}{A_{av} D_{H,av} (\rho_1 + \rho_2)} \right] \tag{19}$$

The friction factor correlation used in equation (19) was the smooth-pipe approximation developed by Koo (ref. 15).

$$f = 0.0014 + 0.125\,Re_c^{-0.32} \tag{20}$$

In order to solve equation (19), Δp was expressed as a function of the static pressures and total temperatures. This was accomplished by combining (a) the equation of state for an ideal gas

$$\rho = \frac{p}{Rt} \tag{21}$$

(b) the relation between static and total temperature

$$T = t \left(1 + \frac{\gamma - 1}{2} M^2 \right) \tag{22}$$

(c) the continuity equation

$$\dot{m} = \rho U A \tag{23}$$

and (d) the definition of the local Mach number for an ideal gas

$$M = \frac{U}{\sqrt{\gamma R t}} \tag{24}$$

Hence, the static temperature was expressed as the following function of total temperature and static pressure.

$$t = f\{T,p\} = \frac{-1 + \sqrt{1 + \frac{4CT}{p^2}}}{\frac{2C}{p^2}} \tag{25}$$

where C is defined as

$$C = \frac{\gamma - 1}{2}\left(\frac{\dot{m}}{A}\right)^2 \frac{R}{\gamma g_c} \tag{26}$$

Substituting equations (21) and (25) into (19) resulted in

$$p_1 = p_2 + \frac{\dot{m}^2 R}{g_c A_{av}}\left[\frac{f\{T_2,p_2\}}{p_2 A_2} - \frac{f\{T_1,p_1\}}{p_1 A_1} + \frac{4f\,\Delta L\, f\{T_2,p_2\} f\{T_1,p_1\}}{A_{av} D_{H,av}\left(p_1 \cdot f\{T_2,p_2\} + p_2 \cdot f\{T_1,p_1\}\right)}\right] \tag{27}$$

Thus, the upstream pressure p_1 was an implicit function of known quantities such as total temperature, downstream static pressure p_2, coolant flow rate, and flow geometry. This function was then solved using an iterative procedure.

Overall heat balance. - For each wall node, a one-dimensional energy balance between the hot gas and the coolant was assumed. The local heat flux through the wall was expressed in each of the following forms:

(a) heat flux from the hot gas to the plug outer surface

$$\frac{Q}{A_w} = h_g(T_{g,rec} - T_{w,o}) + \frac{Q_{rad}}{A_w} \tag{28}$$

(b) conduction through the plug wall

$$\frac{Q}{A_w} = \frac{k_w}{\tau}(T_{w,o} - T_{w,i}) \tag{29}$$

(c) convection from the plug wall to the coolant (i.e., heat picked up by the coolant)

$$\frac{Q}{A_w} = h_{c,eff}(T_{w,i} - T_{c,rec}) = \dot{m}C_p \frac{\Delta T_c}{A_w} \tag{30}$$

By combining equations (28) to (30), the plug wall heat flux can be shown to be

$$\frac{Q}{A_w} = h_{eq}\left(T_{g,rec} - T_{c,rec} + \frac{Q_{rad}}{h_g A_w}\right) \tag{31}$$

where the overall heat-transfer coefficient is given by

$$h_{eq} = \frac{1}{\frac{1}{h_g} + \frac{1}{h_{c,eff}} + \frac{\tau}{k}} \tag{32}$$

Hence, the plug wall temperatures could be solved for by combining equations (28), (30), and (31) to get for the hot-gas side of the outer wall

$$T_{w,o} = T_{g,rec} - \frac{h_{eq}}{h_g}(T_{g,rec} - T_{c,rec}) + \frac{Q_{rad}}{A_w h_g}\left(1 - \frac{h_{eq}}{h_g}\right) \tag{33}$$

and for the coolant side of the outer wall

$$T_{w,i} = T_{c,rec} + \frac{h_{eq}}{h_{c,eff}}\left(T_{g,rec} - T_{c,rec} + \frac{Q_{rad}}{h_g A_w}\right) \tag{34}$$

Since the radiation heat flux Q_{rad}/A_w is a function of the plug wall temperature $T_{w,o}$, an iteration was required between equations (13) and (33) to solve for the outer wall temperature.

The rise in coolant temperature as it passed through each node was calculated by combining equations (30) and (31) to get

$$\Delta T_c = T_2 - T_1 = h_{eq} A_w \frac{\left(T_{g,rec} - T_{c,rec} + \frac{Q_{rad}}{h_g A_w}\right)}{\dot{m}C_p} \tag{35}$$

The hot-gas recovery temperature used in equations (28), (31), (33), and (35) was

$$T_{g,rec} = T_8 \frac{\left(1 + \sqrt[3]{Pr_g}\,\frac{\gamma - 1}{2} M_g^2\right)}{\left(1 + \frac{\gamma - 1}{2} M_g^2\right)} \tag{36}$$

The hot-gas total temperature T_8 used in equation (36) was altered to account for the hot-gas radial temperature profile. This correction as presented in reference 7 gives the following expression for the total temperature near the plug surface:

$$T_8 = 0.894\, T_{8,av} - 36 \qquad (T \text{ in K}) \tag{37a}$$

or

$$T_8 = 0.894\, T_{8,av} - 65 \qquad (T \text{ in } {}^{\circ}R) \tag{37b}$$

Strut Model

Hot-gas pressure, velocity, and temperature distributions. - The hot-gas pressure, velocity, and temperature distributions over the strut were calculated using the potential flow solution for flow over an ellipse (ref. 16). This solution yields the following expressions for the velocity, pressure, and temperature distributions:

$$U_g = \frac{U_\infty}{\left\{\left[\frac{b_1^2}{(a + b_1)\eta}\right]^2 + \left(\frac{a - b_1}{a + b_1}\right)\right\}^{1/2}} \tag{38}$$

$$p_g = p_\infty + \frac{1}{2}\rho_\infty U_\infty^2 \left[1 - \left(\frac{U_g}{U_\infty}\right)^2\right] \tag{39}$$

$$t = t_\infty \left[\frac{2 + (\gamma - 1) M_\infty^2}{2 + (\gamma - 1) M_g^2}\right] \tag{40}$$

where

$$M_g^2 = \frac{2}{\gamma - 1}\left[\left(\frac{p_g}{p_\infty}\right)^{-(\gamma-1)/\gamma} - 1\right] \tag{41}$$

Hot-gas-side heat-transfer coefficient. - The heat-transfer coefficient for the hot-gas side was calculated using the simple pipe-flow equation (1) as suggested by Bartz (ref. 10). The hydraulic diameter in equation (1) was calculated using equations (4) to (6).

Coolant heat-transfer coefficient. - As shown in figure 2, the coolant enters the strut, passes into a central plenum, flows through a series of holes, and impinges on the strut leading-edge region. The coolant then flows parallel to the hot-gas stream through passages formed by fins located between the inner and outer walls. At the strut trailing edge, the coolant enters an exit chamber through another series of holes.

The coolant heat-transfer coefficient used for the leading-edge region was calculated using the impingement correlation developed by Metzger (ref. 17) for impingement cooling of concave surfaces with lines of circular air jets, that is,

$$h_c = 0.355\, G C_p Re_{c,B}^{-0.27}\left(\frac{B}{\zeta}\right)^{0.52} \tag{42}$$

where ζ is the length of the impingement cooled region and B is the width of an equivalent two-dimensional nozzle (slot). The equivalent slot was defined as having a flow area per unit length equal to that of the circular air jets. The actual Reynolds numbers used in the equation were beyond the range of Reynolds numbers investigated by Metzger. Fortunately, however, the total heat flux to the coolant (and hence the wall temperature) was controlled primarily by the hot-gas-side heat-transfer coefficient, and errors in calculating h_c did not significantly change the predicted wall temperatures.

For the finned channels, the heat-transfer coefficient for the walls was calculated using the McAdams correlation for turbulent flow in a pipe (ref. 15) with a correction for curvature

$$h_c = 0.023\, Re_c^{0.8} Pr_c^{0.4}\, C_1 \frac{k_c}{D_H} \tag{43}$$

The effect of curvature C_1 was (ref. 6)

$$C_1 = \left[Re_c\left(\frac{D_H}{2R_{cv}}\right)^2\right]^{0.05} \tag{44}$$

An effective heat-transfer coefficient due to the high conductivity fin was calculated using equation (16).

Coolant pressure distribution. - The coolant pressure distribution was calculated using the same method as for the plug (eqs. (19) to (27)).

RESULTS AND DISCUSSION

A prediction method has been presented for the determination of the pressure and temperature distributions of the convectively air-cooled plug nozzle. Predicted were (1) the hot-exhaust-gas pressure, temperature, and velocity distributions, (2) the strut and plug coolant pressure, temperature, and velocity distributions, and (3) the strut and plug wall temperatures. Comparisons with experimental data and areas requiring further analysis will be discussed herein.

Plug

Figure 5 presents three photographs of the plug nozzle in operation. The test condition for each of the photos are summarized in table II. The secondary cylindrical shroud, not visible in these photographs, was the short, takeoff length. Instrumentation leads are clearly visible on the fixed-area primary shroud. Also, a 10° half-angle conical extension was added to the plug at the 60-percent point. This extension is film cooled with the air discharging from the convective-cooling passages.

These photographs are included to show qualitatively the nonuniform plug wall temperatures, both circumferentially and axially. The circumferential temperature profile, qualitatively illustrated in figure 6, exhibits a regular variation of every $\pi/12$ radians (15°). These variations were apparently caused by the internal cooling configuration (see fig. 2). The fins connecting the plug inner and outer walls served as conduction paths to the cool inner wall, thereby causing locally reduced wall temperatures. Larger circumferential temperature variations exist in noncyclic patterns. These variations apparently were caused by nonuniform coolant flow distributions; the coolant nonuniform flow distributions, in turn, were caused by (1) the interruption of the coolant flow passages in line with the struts, and (2) the presence of instrumentation in many of the coolant channels. The prediction technique presented in this report does not attempt to predict these circumferential temperature variations; the coolant flow rate is assumed to be uniformly distributed in each of the 15° segments.

Significant axial temperature variations can also be seen in figure 5. These variations are caused by the overexpansion and recompression of the supersonic hot gas along the plug surface. A comparison of figures 5(a) to (c) shows that the expansion and com-

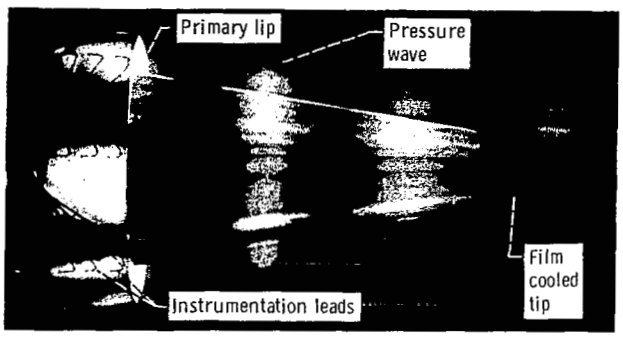

(a) Nozzle pressure ratio, 2.77.

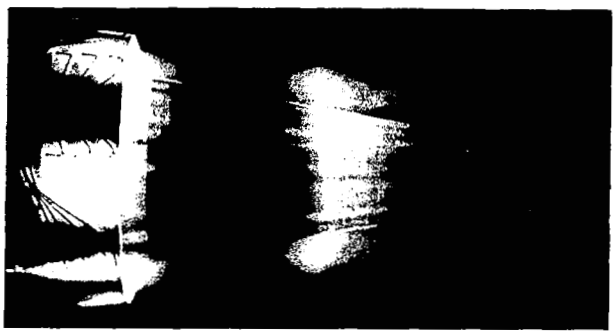

(b) Nozzle pressure ratio, 3.84.

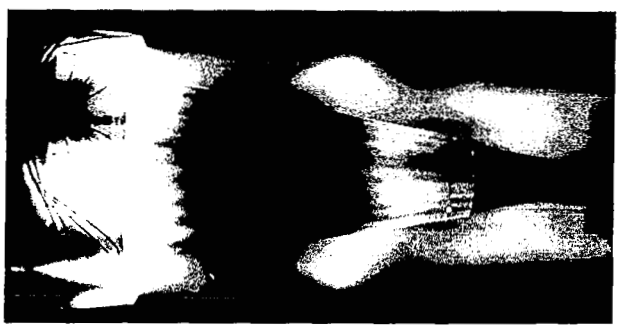

(c) Nozzle pressure ratio, 4.89.

Figure 5. - Plug nozzle in propulsion systems laboratory.

TABLE II. - SUMMARY OF TEST CONDITIONS FOR FIGURE 5

Figure	Nozzle pressure ratio, P_8/p_0	Average exhaust gas total temperature, $T_{8,av}$		Nozzle throat mass flow rate, $\dot{m}_8$		Exhaust gas total pressure, P_8		Coolant flow rate, $\dot{m}_c$, percent of primary	Plug coolant inlet temperature, $T_{c,p,in}$		Average primary nozzle throat wall temperature, $T_{w,8,av}$	
		K	^{o}R	kg/sec	lbm/sec	atm	psia		K	^{o}R	K	^{o}R
5(a)	2.77	1853	3335	16.72	36.9	1.605	23.6	3.93	650	1170	978	1760
5(b)	3.84	1830	3295	15.08	33.3	1.429	21.0	3.84	649	1169	971	1748
5(c)	4.89	1853	3336	19.98	44.1	1.891	27.8	4.02	634	1142	976	1757

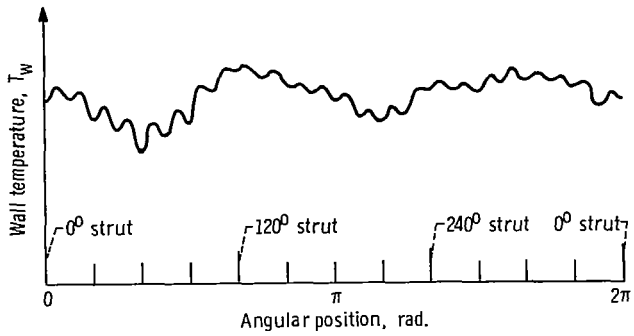

Figure 6. - Qualitative circumferential wall temperature profile.

pression waves (pressure waves) move along the plug surface as the nozzle pressure ratio is varied. Thus, the plug wall axial temperature distribution changes with changing nozzle pressure ratio. To predict these axial temperature variations, the designer must first be able to predict the magnitude of the overexpansions and recompressions; that is, the local pressure distribution. A method has been developed (ref. 4) for fully expanded flow (pressure ratios $> \sim 10$) on a conical plug surface with secondary flow, but no known analytical method exists in the literature for low nozzle-pressure ratios. The designer then is left with two choices: He may run model tests of the nozzle configuration and measure local pressures for various pressure ratios. These local pressures can then be used to predict local wall temperatures. Or he may estimate the local pressure distribution, using isentropic flow equations, realizing that the actual static-pressure distribution will be, in some cases, significantly different than predicted. The temperature differences that can be expected between these two alternative design approaches will be discussed in this report.

Some infrared photographs were also taken of the plug nozzle during the same series of tests. The infrared film was processed as discussed in reference 18. Figure 7 shows the results of one of the infrared pictures. The infrared photographic image is shown in the upper right hand corner of figure 7. The picture was taken through a quartz viewport in the side of the altitude chamber with a manually held camera. View A-A shows the line of sight of the viewport and indicates the region of the plug that should yield reasonable accurate infrared temperature measurements. These temperature contours are shown in figure 7. The test conditions for this infrared photograph are given in table II and are the same as for the photograph shown in figure 5(a) ($P_8/p_0 = 2.77$). The technique produces a very detailed contour map of film density that can be readily converted into temperature contours. Notice that the hot spot on the plug (1090 K (1960° R)) is not located on the 0° or 60° planes of wall temperature thermocouples.

Figures 5 to 7 illustrate the difficulty of trying to predict local wall temperatures. The local variations should be kept in mind when assessing the comparison between predicted and experimental (thermocouples) wall temperature that follow.

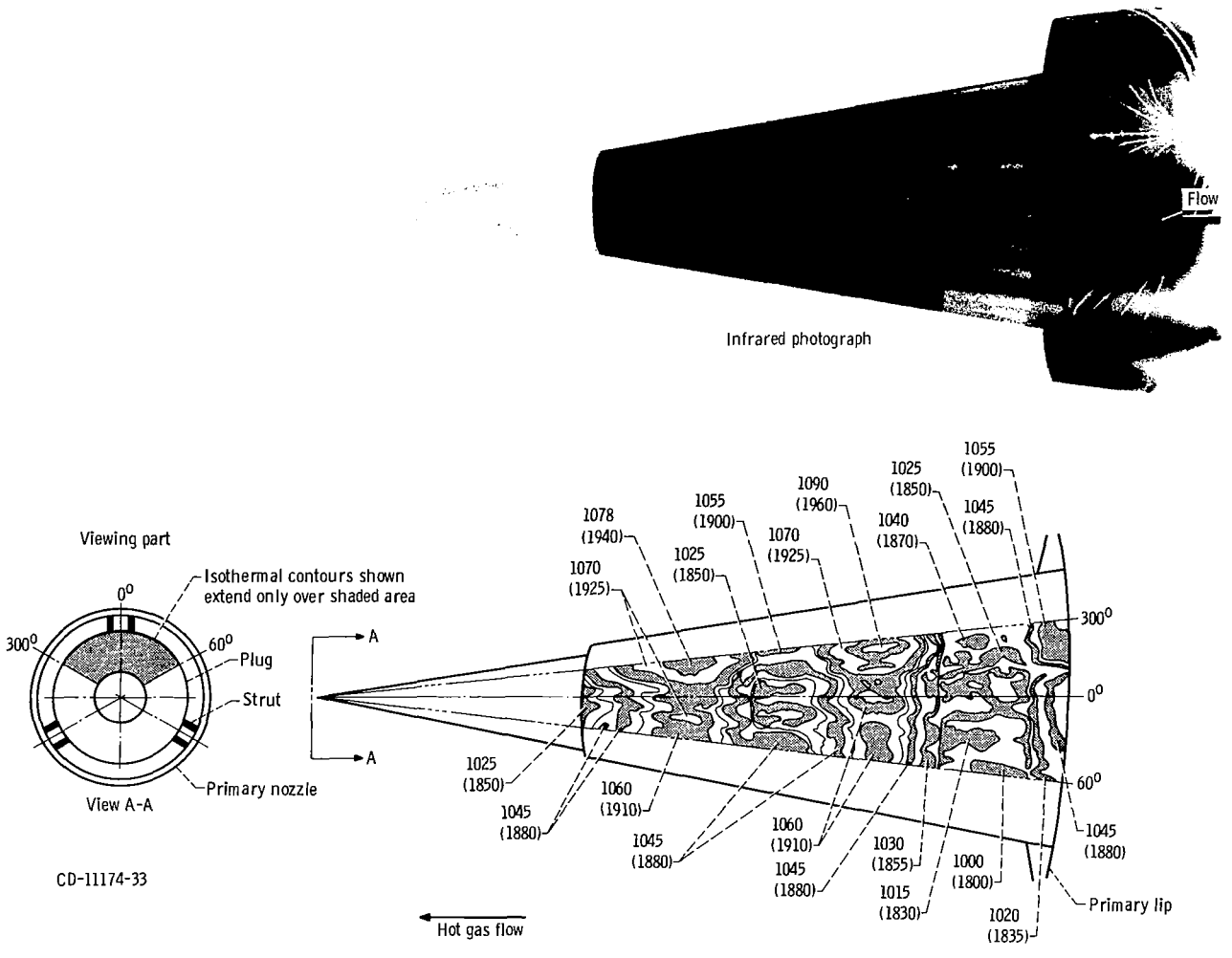

Figure 7. - Isothermal contours (K(^{o}R)) obtained using infrared photographs. Nozzle pressure ratio, 2.77.

Hot-gas static-pressure distribution. - Figure 8(a) presents a comparison of predicted and experimental hot-gas static-pressure distributions for a typical high nozzle-pressure-ratio case ($P_8/p_0 > 10$). The test conditions for this figure and all following figures are given in tables III to V. Isentropic flow equations were used to predict static pressures upstream of the nozzle throat; the analytical procedure of Anderson was used on the supersonic side of the throat. Agreement between the predicted pressure and the experimental data is excellent.

Figure 8(b) presents a similar curve for a typical low nozzle-pressure-ratio case ($P_8/p_0 = 3.22$). For the low nozzle-pressure-ratio case isentropic flow relations were used to predict static pressures on the subsonic side of the nozzle throat and on the supersonic side until the hot-gas pressure equalled the back pressure. Then the pressure was assumed to remain equal to the back pressure to the end of the plug. This ap-

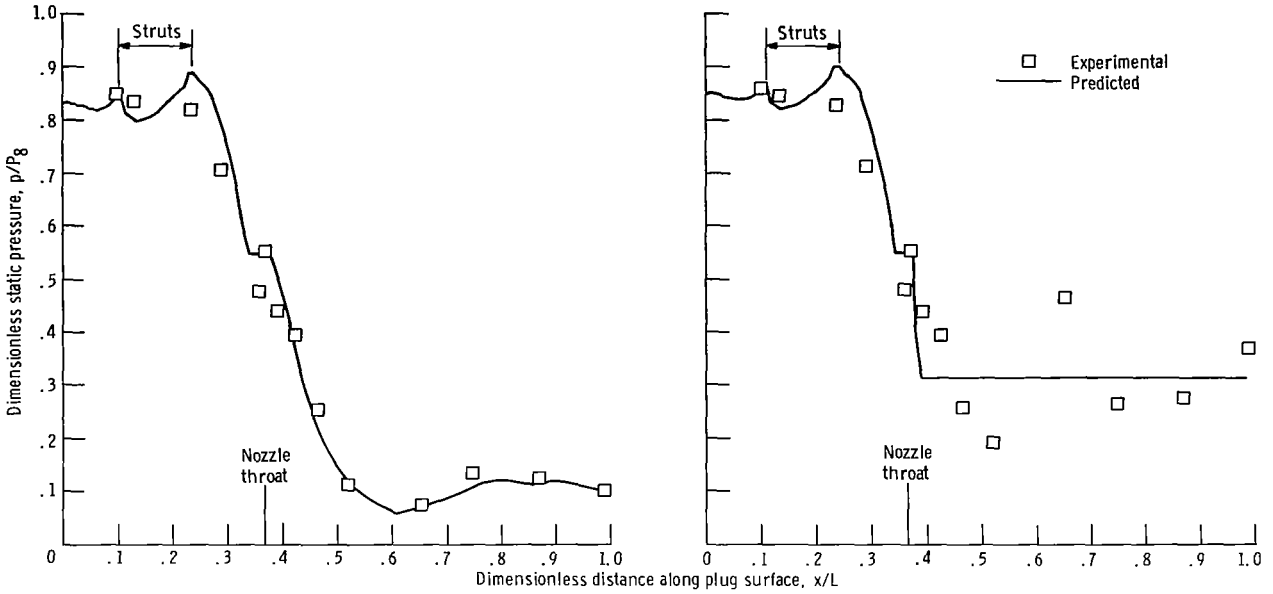

(a) Nozzle pressure ratio, 11.8.

(b) Nozzle pressure ratio, 3.22.

Figure 8. - Comparison of experimental and predicted hot-gas pressures for typical high and low nozzle-pressure-ratio cases.

TABLE III. - OPERATING CONDITIONS FOR TYPICAL RUNS ANALYZED

Nozzle pressure ratio, P_8/p_0	Average exhaust gas total temperature, $T_{8,av}$		Nozzle throat mass flow rate, $\dot{m}_8$		Exhaust gas total pressure, P_8		Coolant flow rate, $\dot{m}_c$, percent of primary	Plug coolant inlet temperature, $T_{c,p,in}$		See figure -
	K	°R	kg/sec	lbm/sec	atm	psia		K	°R	
11.8	1719	3095	20.78	45.82	2.01	29.57	2.66	474	854	8(a), 11(a), 12(a), 14(a), and 15(a)
3.22	1551	2792	20.73	45.58	1.96	28.76	2.29	473	851	8(b), 9, 11(b), 12(b), 13, 14(b), and 15(b)
6.27	1729	3112	21.53	47.46	2.01	29.61	2.72	478	861	16(a)
34.0	1297	2334	19.90	43.88	1.99	29.28	3.16	394	709	16(b)
10.78	1347	2424	21.12	46.57	1.78	26.19	1.88	448	807	17

TABLE IV. - OPERATING CONDITIONS FOR RUNS PLOTTED IN FIGURE 10

Nozzle pressure ratio, P_8/p_0	Average exhaust gas total temperature, $T_{8,av}$		Nozzle throat mass flow rate, $\dot{m}_8$		Exhaust gas total pressure, P_8		Coolant flow rate, $\dot{m}_c$, percent of primary	Plug coolant inlet temperature, $T_{c,p,in}$	
	K	^{o}R	kg/sec	lbm/sec	atm	psia		K	^{o}R
96.7	1358	2445	21.0	46.3	1.78	26.2	1.97	426	766
94.2	1353	2436	21.2	46.6	1.79	26.3	1.49	453	815
82.5	1678	3021	21.6	47.6	2.01	29.5	2.61	457	823
82.4	1725	3105	21.5	47.3	2.01	29.6	2.26	472	850
68.2	1334	2401	21.0	46.3	1.78	26.1	2.35	409	737
48.6	1633	2940	10.8	23.8	.99	14.5	2.66	456	820
38.6	1594	2870	10.4	23.0	.93	13.7	2.56	458	824
22.3	1709	3076	21.5	47.3	2.00	29.4	2.58	456	820
22.0	1382	2489	21.1	46.4	1.79	26.3	2.35	411	739
21.5	1341	2414	21.1	46.5	1.78	26.1	1.56	443	798
11.8	1719	3095	21.5	47.3	2.01	29.6	2.27	474	854
10.9	1353	2436	21.2	46.6	1.78	26.2	2.32	413	743
10.7	1348	2426	21.1	46.4	1.78	26.1	1.98	429	773
[a]8.20	1571	2828	19.9	43.8	1.82	26.8	3.74	591	1063
[a]7.21	1769	3184	19.9	43.9	1.90	28.0	3.63	599	1079
[a]6.59	1448	2607	19.7	43.5	1.75	25.7	3.68	575	1035
6.27	1733	3120	21.5	47.3	2.01	29.6	2.80	464	836
[a]5.74	1708	3075	19.0	41.8	1.78	26.2	3.63	607	1092
5.69	1469	2644	21.3	46.9	1.84	27.0	1.60	468	842
5.67	1392	2505	21.4	47.1	1.83	26.9	2.28	433	779
3.22	1551	2792	21.7	47.8	1.96	28.8	1.88	473	851
3.17	1523	2741	21.7	47.8	1.93	28.4	3.55	406	730

[a]Runs using compressor bleed air as the coolant.

TABLE V. - OPERATING CONDITIONS FOR RUNS PLOTTED IN FIGURE 18

Nozzle pressure ratio, P_8/p_0	Average exhaust gas total temperature, $T_{8,av}$		Nozzle throat mass flow rate, $\dot{m}_8$		Exhaust gas total pressure, P_8		Coolant flow rate, $\dot{m}_c$, percent of primary	Plug coolant inlet temperature, $T_{c,p,in}$	
	K	^{o}R	kg/sec	lbm/sec	atm	psia		K	^{o}R
5.66	1432	2578	20.63	45.49	1.83	26.85	2.12	314	566
5.69	1500	2700	20.63	45.50	1.83	26.97	1.91	316	568
6.27	1766	3178	20.86	45.99	2.01	29.61	2.72	316	569
6.27	1771	3187	20.80	45.86	2.01	29.60	3.11	313	564
10.61	1366	2459	20.53	45.27	1.76	25.93	2.67	303	546
10.72	1367	2461	20.60	45.42	1.78	26.11	2.29	305	549
10.78	1365	2457	20.67	45.57	1.78	26.19	1.88	307	552
34.0	1297	2334	19.90	43.88	1.99	29.28	3.16	297	535

proximation (fig. 8(b)) yields a reasonable average pressure on the plug surface, but significant differences can be seen in local values. The effect of this approximation is seen in figure 9. The solid lines on the figure represent the predicted plug outer wall temperature with the local velocities calculated from the predicted pressure distribution shown in figure 8(b). The dashed lines in the figure were calculated using the measured static pressures (and linearly interpolating between them). The dashed lines appears to follow the experimental data more closely, as expected, but the difference between the two predicted curves is small (about 30 K (54° R)). A similar comparison was made in reference 7, with essentially the same results. Thus, the constant pressure assumption on the supersonic plug surface can be used for this pressure ratio with little error introduced. Similar results were obtained for the high nozzle-pressure-ratio cases. Therefore, the assumption of isentropic expansion to constant back pressure should yield reasonable design results for all pressure ratios.

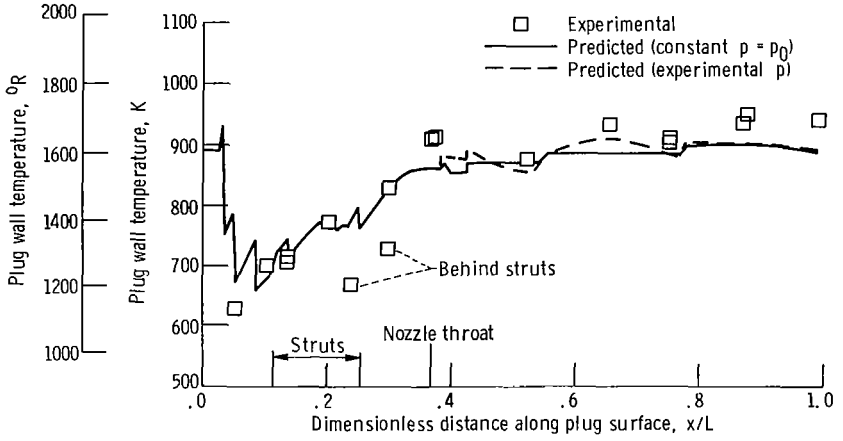

Figure 9. - Effect of hot-gas pressure distribution on predicted wall temperatures and data comparison for typical low nozzle-pressure-ratio case (P_8/p_0 = 3.22). Bartz-Boldman heat-transfer-coefficient hg calculation used in both predictions.

The static pressures in the subsonic region of the nozzle from x/L = 0.1 to the throat were first underpredicted and then overpredicted (figs. 8 and 9). The deviation from isentropic flow was probably caused by the struts in this region. Near the leading edge, entrance region effects account for the local pressure being higher than the isentropic flow equations predict it to be. As the gas flows around the struts, a hydrodynamic boundary layer builds up and eventually separates from the strut surface. The re-

sulting vortex streets created a reduction in the effective flow area and hence an increase in velocity and a decrease in static pressure.

Coolant temperature distribution. - Figure 10 compares the predicted coolant temperature rise with measured temperature rise for a representative sample of cases. Two thermocouples measured the coolant inlet temperature, 12 thermocouples measured the coolant temperature at the nozzle primary throat, and 12 thermocouples measured the coolant temperature at the coolant channel exit. The open symbols in figure 10 indicate the temperature rise from the inlet to the throat, and the closed symbols indicate the temperature rise from the inlet to the cooling channel exit.

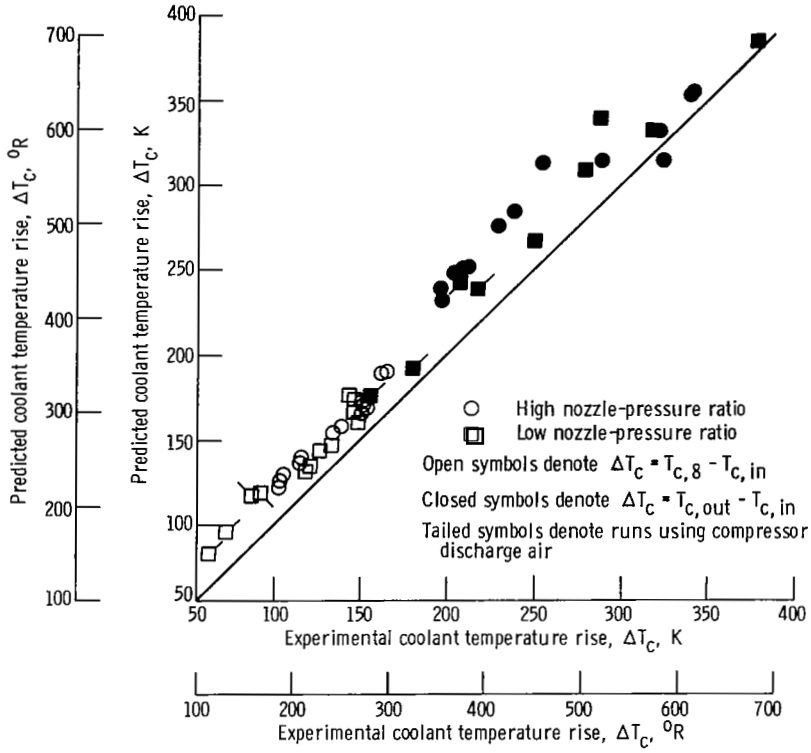

Figure 10. - Comparison of experimental and predicted coolant temperature rise.

The temperature rise from the inlet to the primary nozzle throat was consistently about 22.2 K (40° R) overpredicted. There are at least two possible explanations for this overprediction: (1) The plug inner wall was assumed to be adiabatic, but was probably giving up heat to the cool air circulating inside the plug. (2) As noted in reference 1, a small air leak existed between the nose cap and the plug at the plug leading edge. This air obviously film cooled the plug some in this region of the plug (i.e., insulated the plug from the hot gas for a short distance). This film cooling was neglected in the prediction.

This leak was apparently very small, however, because there was no significant drop in wall temperature downstream of the leak.

The overprediction of coolant temperature rise from the inlet to the end of the coolant channels was only slightly more than 22.2 K (40° R) (with more data scatter, however). This indicates that heat may have been transferred across the assumed adiabatic inner wall. The prediction was felt to be satisfactory; efforts to improve the prediction failed because the coolant flow paths within the plug cavity were unknown. Also, an accelerometer was mounted in the base of the plug (see fig. 3) and required air cooling. The cooling-air flow rate and temperature to the accelerometer were measured, but the temperature of the air leaving the accelerometer was not. Thus, a heat balance on the air in the plug inside cavity was not possible.

Coolant pressure distributions. - Figure 11 compares predicted and experimental coolant static pressures as a function of distance along the plug surface for typical high and low nozzle-pressure ratios. The agreement is excellent.

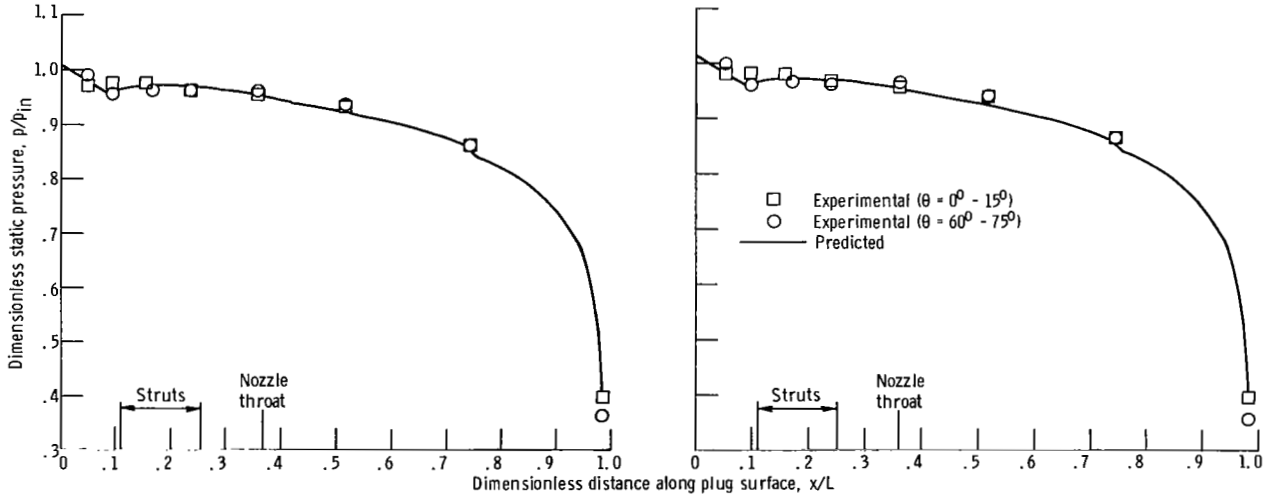

(a) Nozzle pressure ratio, 11.8.

(b) Nozzle pressure ratio, 3.22.

Figure 11. - Comparison of experimental and predicted coolant pressures for typical high and low nozzle-pressure-ratio cases.

Plug wall temperatures. - Figure 12 compares predicted and experimental data for the plug wall temperature and coolant temperature as a function of distance along the plug surface for a typical high and low pressure ratios cases. In figure 12(a), the plug wall temperature predicted using the Bartz-Boldman heat-transfer coefficient (solid line) is in excellent agreement with the measured wall temperatures. At the critical primary throat station, the maximum wall temperature around the plug circumference is underpredicted by about 69 K (125° R).

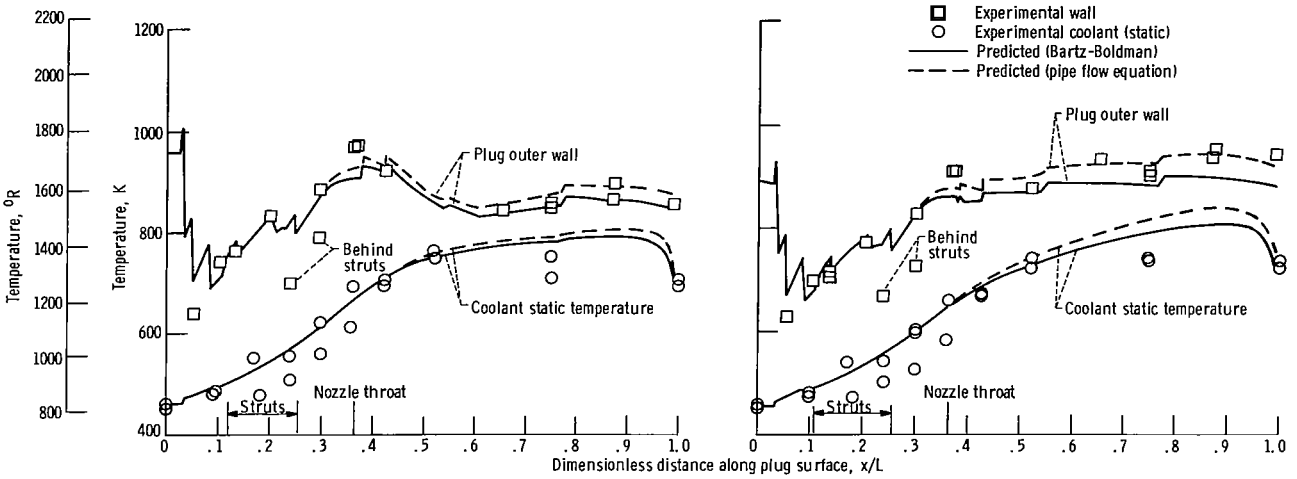

(a) Nozzle pressure ratio, 11.8.

(b) Nozzle pressure ratio, 3.22.

Figure 12. - A comparison of experimental and predicted plug wall and coolant temperatures for typical high and low nozzle-pressure-ratio cases.

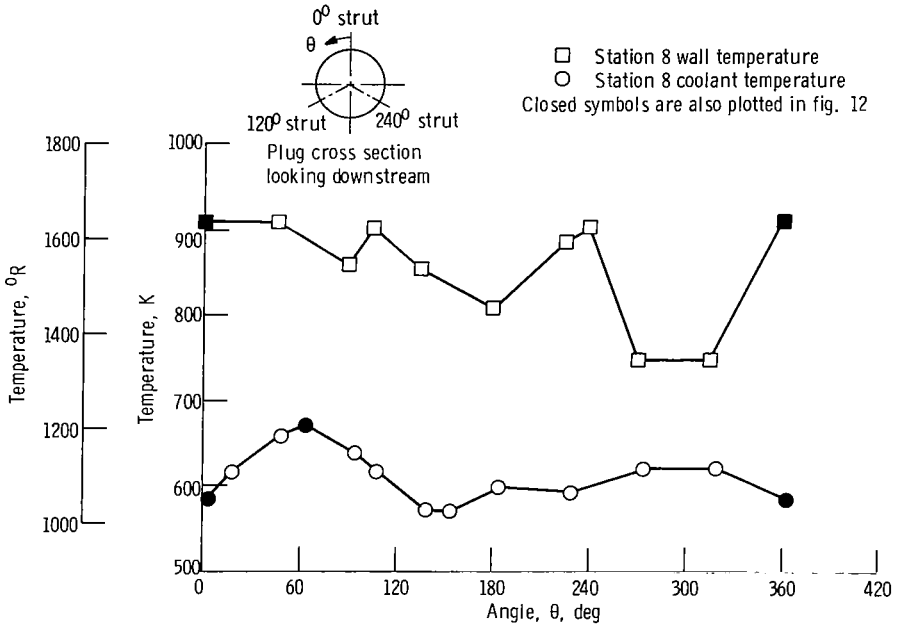

Figure 13. - Circumferential variation of the plug wall and coolant temperatures. Nozzle pressure ratio, 3.22.

For the low pressure-ratio case (fig. 12(b) agreement between predicted and experimental temperatures is excellent in the subsonic region of the plug. The plug throat temperature is underpredicted by about 50 K (90° R). Figure 13 presents the measured (thermocouple data) circumferential plug wall and coolant temperature variation for a typical case. Differences as high as 160 K (288° R) are noted in wall temperature and 100 K (180° R) in coolant temperature. The closed symbols in figure 13 are the data plotted in figure 12(b) at x/L = 0.37. Obviously, the predicted wall temperature is well within the circumferential variation in measured wall temperature.

On the supersonic side of the primary throat (fig. 12(b), the Bartz-Boldman technique tends to result in an underprediction of the wall temperatures at large x/L. A pipe-flow equation (ref. 11) for calculating the hot-gas heat-transfer coefficient was also investigated. The hot gas was assumed to remain attached to the plug and the areas (and hydraulic diameter) were calculated to match, isentropically, the predicted local pressures. The resulting heat-transfer coefficients were higher than the Bartz-Boldman coefficients as shown in figure 14. Predicted wall temperatures using the pipe-flow equation heat-transfer coefficients are presented as the dashed lines in figure 12. For the high pressure-ratio case (fig. 12(a)) either method can be used with confidence. For the low pressure-ratio case (fig. 12(b)) the pipe-flow equation appears to yield better results. For a designer the pipe-flow equation offers two advantages: (1) it is easier to use, and (2) wall temperatures predicted using the pipe-flow equation tend to be slightly more conservative (i.e., higher) than the Bartz-Boldman results, in the supersonic region.

The driving temperature used with both the Bartz-Boldman and pipe-flow heat-transfer coefficients was the hot-gas total temperature near the plug surface (see

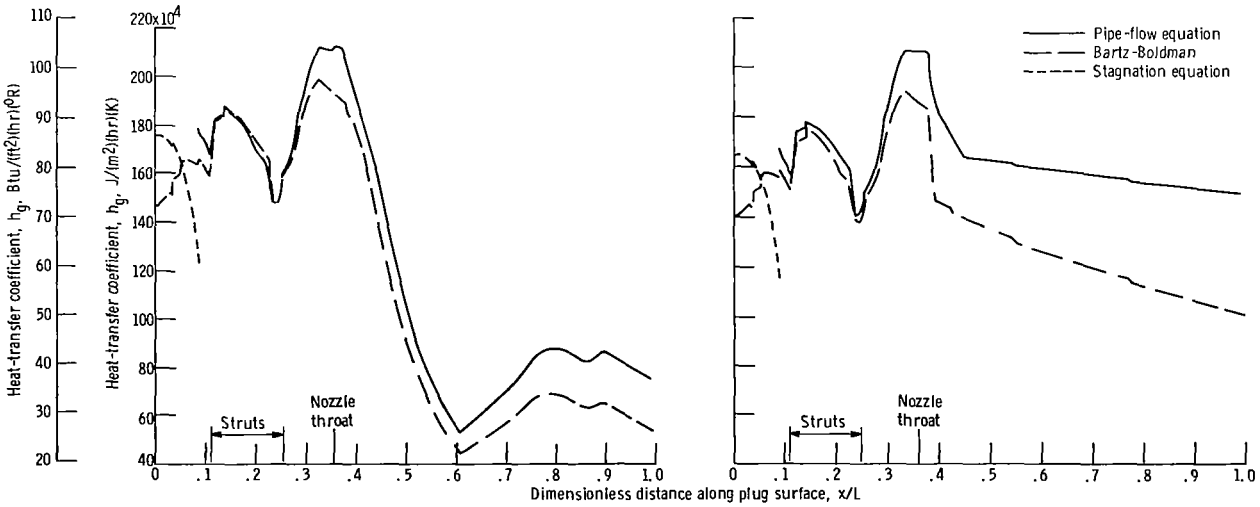

(a) Nozzle pressure ratio, 11.8 (b) Nozzle pressure ratio, 3.22.

Figure 14. - Calculated hot-gas-side heat-transfer coefficients for typical high and low nozzle-pressure-ratio cases.

eqs. (37a) and (37b)). This near-the-surface temperature was approximated using radial hot-gas temperature profiles measured just beyond the nozzle throat (ref. 7). Another possible driving temperature as suggested in reference 7 was the radially averaged hot-gas total temperature $T_{8,av}$. Using this temperature in the prediction scheme resulted in predicted plug wall temperatures which were about 10 percent higher than the experimental data over the entire plug length.

Heat-flux distributions. - Predicted heat-flux distributions for the high and low pressure-ratio cases are shown in figure 15. Convection heat transfer from the gas to the wall is the primary heating mechanism over the entire plug surface. Flame radiation adds a small amount of heat to the wall and radiation from the plug to the altitude chamber cools the plug downstream of the primary nozzle throat.

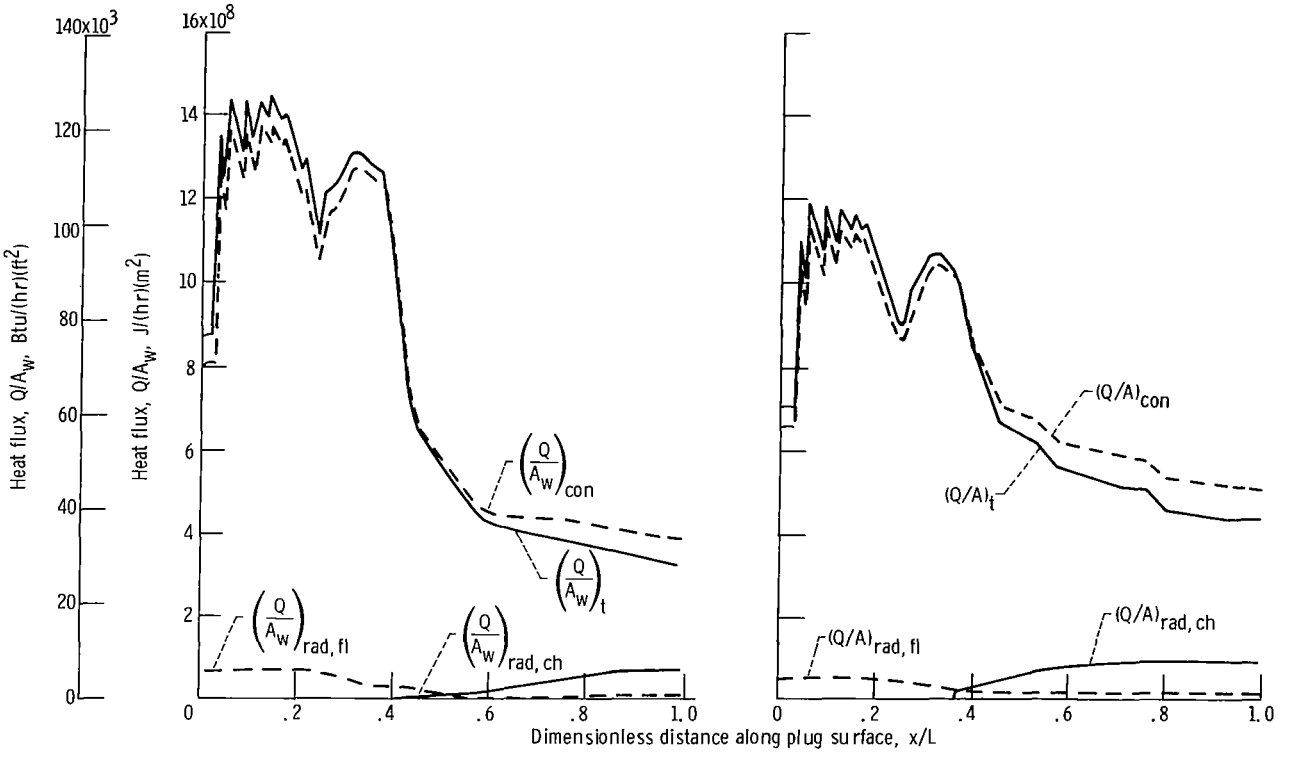

(a) Nozzle pressure ratio, 11.8.

(b) Nozzle pressure ratio, 3.22.

Figure 15. - Calculated convection and radiation heat flux-distributions for typical high and low nozzle-pressure-ratio cases.

Struts

The strut cooling airflow paths are shown in figure 2. As discussed in reference 1, a large radial temperature gradient existed in the primary gas stream. This profile was neglected in the strut analysis; an average gas total temperature was used.

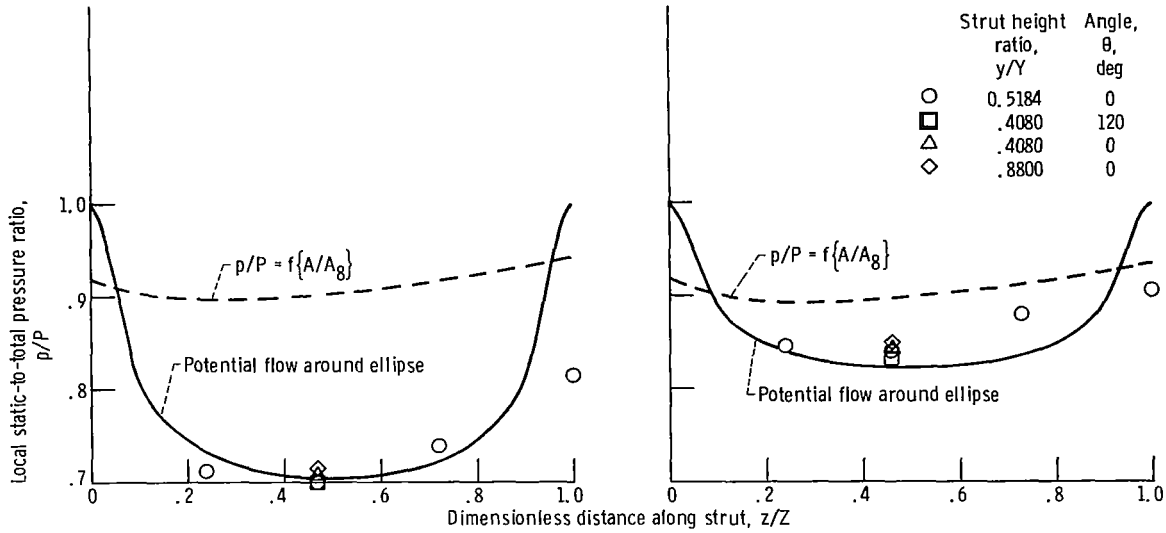

(a) High flow rate case.

(b) Low flow rate case.

Figure 16. - Hot-gas pressure distribution on strut.

Hot-gas pressure distribution. - Figure 16 presents a comparison of predicted and experimental pressures on the struts for a typical high primary flow rate (fig. 16(a)) and a typical low primary flow rate (fig. 16(b)). In each case the measured and predicted pressures are in good agreement over most of the strut surface. At the strut trailing edge the measured pressure is lower than the predicted value. This difference can be attributed to separation.

Strut wall temperature. - Figure 17 presents typical experimental strut wall and coolant temperatures and the predicted temperatures. The experimental wall temperatures generally follow the pattern shown in this figure: cool at the leading edge, hot at the midchord and cooler again at the trailing edge. In the spanwise direction, the wall temperature follows the gas temperature profile: cool near the plug, hot at midspan, and cooler again at the primary shroud. A comparison of the average measured wall temperature at the leading edge and midchord with the predicted temperature yields reasonably close agreement. Comparisons at the trailing-edge thermocouple station are not as good but are probably caused by both local separations of the primary flow-condition losses through the fins to the support structure (see fig. 2).

A comparison of predicted and measured coolant temperatures is also given in figure 17 and, on the average, the prediction appears to be reasonable. Figure 18 compares the predicted and measured coolant temperature rise in the struts for several runs. Again, the measured and predicted values are close. The largest difference noted is about 10 K (18° R).

A nozzle designer would undoubtedly design the afterburner to yield a gas temperature profile similar to the profile studied herein; cool on the nozzle centerline and near

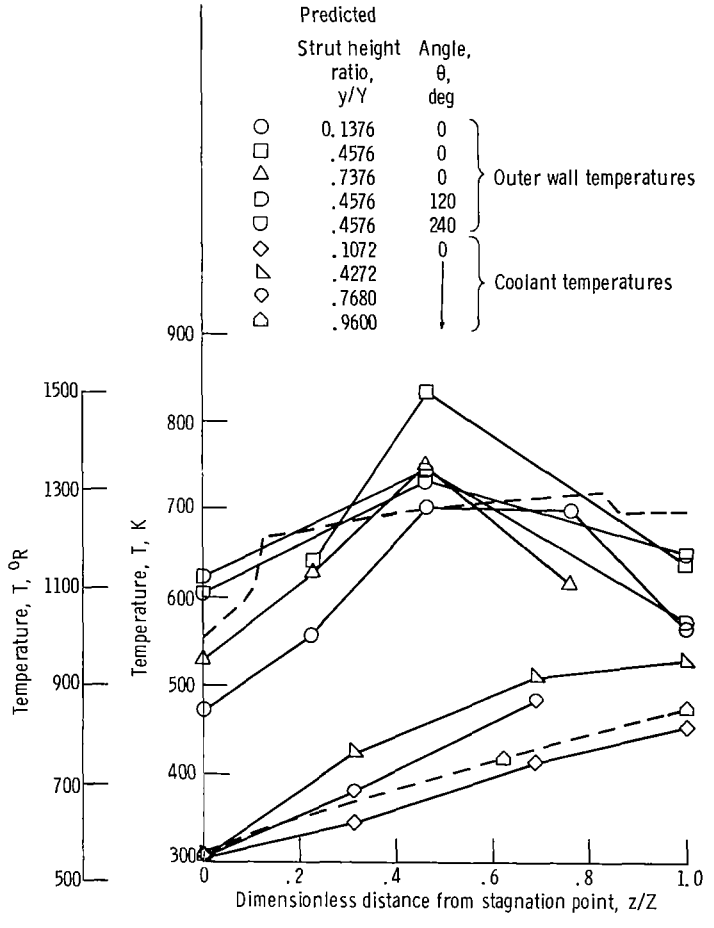

Figure 17. - Strut temperature distribution.

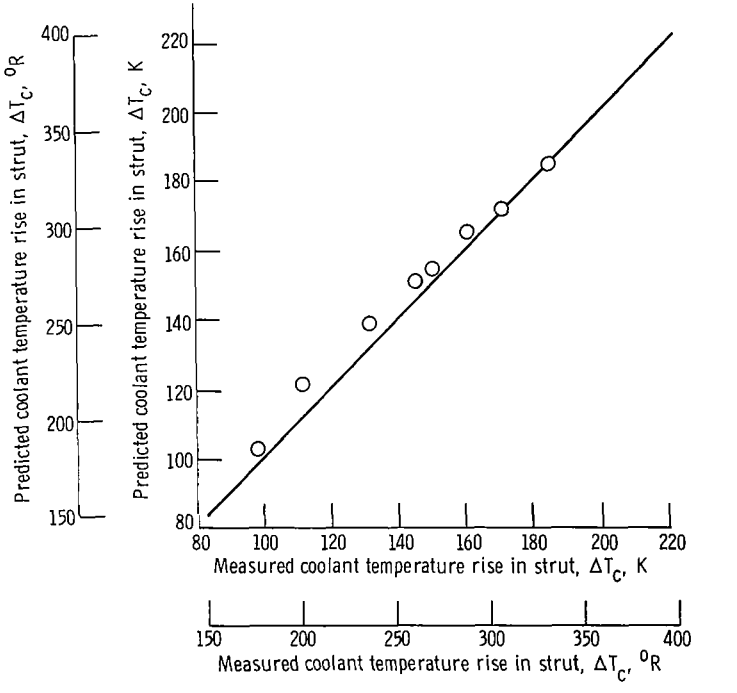

Figure 18. - A comparison of experimental and predicted coolant temperature rise from leading to trailing edge of strut.

the primary wall and hot between these two regions. Since this hot region of the primary stream can cause local hot spots on a strut inserted in the stream, a more practical technique might be to attach the plug to the engine through a string support, which itself is surrounded by the coolest region of the gas stream. This approach should reduce the coolant requirements for the nozzle system (ref. 7).

SUMMARY OF RESULTS

A prediction technique is outlined for the calculations of temperature and pressure distribution of a plug nozzle and supporting struts. The nozzle studied was designed for operation in an afterburning turbojet engine and was convectively air cooled using engine compressor air. Comparisons of experimental data with predicted results are summarized below:

1. The method of Anderson yields excellent predictions of static pressure on the supersonic plug surface for nozzle pressure ratios greater than about 10. Isentropic flow relations yield reasonable results in the subsonic flow regime.

2. For low nozzle-pressure ratios differences in predicted wall temperatures of less than 30 K (54° R) were found between (a) assuming one-dimensional isentropic expansion to back pressure and constant pressure thereafter, and (b) using the measured pressure profiles. Similar results were obtained for higher pressure ratios.

3. The prediction technique generally overpredicted the plug coolant temperature rise by slightly more than 22 K (40° R). This overprediction may have been caused by (a) a small leak around the plug nose cap that was not considered in the analysis or (b) a convective heat loss to the air in the plug inner cavity.

4. The prediction technique calculates the coolant pressure distribution very well.

5. Either the Bartz-Boldman integral boundary-layer technique or a simple pipe-flow equation may be used to calculate heat-transfer coefficients and, hence, plug wall temperatures. The pipe-flow equation is easier to use, however, and results in slightly more conservative (higher) wall temperatures.

6. The driving temperature used in the heat-transfer calculations was the total temperature of the hot gas near the plug wall. This temperature may be used with both the Bartz-Boldman and pipe-flow heat-transfer coefficients. Using the average gas temperature as the driving temperature results in wall temperatures that are about 10 percent higher than experimental data.

7. The potential flow prediction technique yielded a good prediction of static pressure over most of the strut surface. The prediction of strut wall temperature was reasonable at the strut leading edge and in the midchord region, but the prediction was high at the trailing edge. The coolant temperature rise was predicted to within about 10 K (18^{O} R).

Lewis Research Center,
National Aeronautics and Space Administration,
Cleveland, Ohio, January 24, 1972,
764-74.

APPENDIX - SYMBOLS

A	area
a	semimajor axis of strut cross section
B	width of an equivalent two-dimensional nozzle
b	fin thickness
b_1	semiminor axis of strut cross section
C	factor in eq. (26)
C_1	curvature correction factor (eq. (44))
c_p	specific heat
D	diameter
D_H	hydraulic diameter
D_0	diameter of plug leading edge region
d	flow field thickness
F	radiation shape factor
Fa	fuel-air ratio
f	Fanning friction factor
f{ }	function notation
G	mass flow rate per unit area
g_c	gravitational conversion factor
h	heat-transfer coefficient
k	thermal conductivity
L	length
l	fin length
M	Mach number
$\dot{m}$	mass flow rate
P	total pressure
Pr	Prandtl number
$\mathscr{P}$	perimeter

p	static pressure
Q	heat flow rate
R	specific gas constant
R_{cv}	radius of curvature
Re	Reynolds number
r	radius
r'	radius of flow-field outer boundary
S	fin center-to-center spacing
T	total temperature
t	static temperature
U	velocity
x	plug surface coordinate
Y	strut height (see fig. 4)
y	strut height coordinate
Z	total strut surface distance
z	strut surface coordinate
α	radiation angle (see fig. 4)
β	angle (see fig. 4)
γ	ratio of specific heats
ϵ	emissivity
ζ	length of impingement cooled region
η	local strut coordinate (see fig. 4, section B-B)
θ	angle (fig. 4)
ξ	characteristic length
ρ	density
σ	Stefan-Boltzmann constant
τ	plug wall thickness

Subscripts:

av	average
c	coolant

ch	exhaust chamber wall
con	convective
eff	effective
eq	equivalent or overall
f	fin
fl	flame
g	hot gas
i	inside
imp	impingement tube
in	coolant inlet station
o	outside
out	coolant exit station
p	plug
r	reference
rad	radiation
rec	recovery
st	strut
t	total
w	wall
1	upstream station index
2	downstream station index
8	primary nozzle throat
0	ambient
∞	free stream

REFERENCES

1. Clark, John S.; Graber, Edwin J.; and Straight, David M.: Experimental Heat Transfer and Flow Results from an Air-Cooled Plug Nozzle System. NASA TM X-52897, 1970.

2. Huntley, Sidney C.; and Samanich, Nick E.: Performance of a 10^{o} Conical Plug Nozzle Using a Turbojet Gas Generator. NASA TM X-52570, 1969.

3. Darchuk, George V.; and Balombin, Joseph R.: Noise Evaluation of Four Exhaust Nozzles for Afterburning Turbojet Engine. NASA TM X-2014, 1970.

4. Beheim, Milton A.; Anderson, Bernhard H.; Clark, John S.; Corson, Blake W., Jr.; Stitt, Leonard E.; and Wilcox, Fred A.: Supersonic Exhaust Nozzles. Aircraft Propulsion. NASA SP-259, 1971, pp. 233-282.

5. Shapiro, Ascher H.: The Dynamics and Thermodynamics of Compressible Fluid Flow. Vol. 1. Ronald Press Co., 1953.

6. Rohde, John E.; Duscha, Rudolph A.; and Derderian, George.: Digital Codes for Design and Evaluation of Convectively Cooled Rocket Nozzle with Application to Nuclear-Type Rocket. NASA TN D-3798, 1967.

7. Clark, John S.; and Lieberman, Arthur: Thermal Design Study of an Air-Cooled Plug-Nozzle System for a Supersonic-Cruise Aircraft. NASA TM X-2475, 1971.

8. Kreith, Frank: Principles of Heat Transfer. International Textbook Co., 1958.

9. Cary, John R.: The Determination of Local Forced-Convection Coefficients for Spheres. Trans ASME, vol. 75, no. 4, May 1953, pp. 483-487.

10. Bartz, D. R.: A Simple Equation for Rapid Estimation of Rocket Nozzle Convective Heat Transfer Coefficients. Jet Propulsion, vol. 27, no. 1, Jan. 1957, pp. 49-51.

11. Boldman, Donald R.; Neumann, Harvey E.; and Schmidt, James F.: Heat Transfer in 30^{o} and 60^{o} Half-Angle of Convergence Nozzles with Various Diameter Uncooled Pipe Inlets. NASA TN D-4177, 1967.

12. Anon.: Computer Program for the Analysis of Annular Combustors. Vol. I - Calculation Procedures. Report No. 1111-1, vol. 1, Northern Research and Engineering Corp. (NASA CR-72374), Jan. 29, 1968.

13. Gordon, Robert; and Cobonpue, John: Heat Transfer Between a Flat Plate and Jets of Air Impinging on It. International Developments in Heat Transfer. ASME, 1963, pp. 454-460.

14. Vennard, John K.: Elementary Fluid Mechanics. Third ed., John Wiley & Sons, Inc., 1954.

15. McAdams, William H.: Heat Transmission. Second ed., McGraw-Hill Book Co., Inc., 1942.

16. Rauscher, Manfred: Introduction to Aeronautical Dynamics. John Wiley & Sons, Inc., 1953.

17. Metzger, D. E.; Yamashita, T.:, and Jenkins, C. W.: Impingement Cooling of Concave Surfaces with Lines of Circular Air Jets. Paper 68-WA/GT-1, ASME, Dec. 1968.

18. Pollack, Frank G.; and Hickel, Robert O.: Surface Temperature Mapping with Infrared Photographic Pyrometry for Turbine Cooling Investigations. NASA TN D-5179, 1969.

NASA-Langley, 1972 — 33 E-6709